Food Chemistry: X 15 (2022) 100361

Contents lists available at ScienceDirect

Food Chemistry: X

journal homepage: www.sciencedirect.com/journal/food-chemistry-x

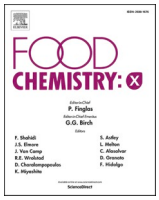

Preparation and characterization of garlic polysaccharide-Zn (II) complexes and their bioactivities as a zinc supplement in Zn-deficient mice

Xinyan Bai, Zhichang Qiu, Zhenjia Zheng, Shuoshuo Song, Renjie Zhao, Xiaoming Lu *, Xuguang Qiao *

Key Laboratory of Food Processing Technology and Quality Control of Shandong Higher Education Institutes, College of Food Science and Engineering, Shandong Agricultural University, 61 Daizong Street, Tai'an, Shandong 271018, PR China

ARTICLE INFO

Keywords:
Polysaccharide-Zn (II) complex
Preparation
Structural characterization
Zinc supplement

ABSTRACT

This study explored the potential of garlic polysaccharides (GPs) as a carrier for synthesizing GP-Zn (II) complexes to supplement Zn. According to the response surface analysis, the optimal preparation conditions were: mass ratio of GPs to Zn^{2+} 1:0.21, temperature 53 °C, pH 5.9 and time 148.75 min, with the maximum chelation rate of 90.11%. The chelation of GPs and Zn^{2+} involved O—H/C—O/O—C—O groups, increased crystallinity and altered absorption peaks of circular dichroism spectra, with a higher thermal stability, particle size and negative zeta potential. Compared with inorganic zinc salts, supplementation of GP-Zn (II) complexes showed enhance zinc supplementation effects in Zn-deficient mice model: increased body weight, organ index and Zn (II) levels in serum and liver, enhanced Superoxidedismutase (SOD) activity and alkaline phosphatase activity, decreased NO content and Malondialdehyde (MDA) content and improved colon and testicular morphology. Therefore, GP-Zn (II) complex can be used as a potential zinc supplement for Zn-deficient individuals.

1. Introduction

Zinc is an essential trace element widely present in the human body (Outten & O'Halloran, 2001). It is not only associated with metabolic processes (e.g. cell growth, division and proliferation) but also involved in the biosynthesis of >300 enzymes in the body, including superoxide dismutase (SOD), alcohol dehydrogenase and alkaline phosphatase (ALP) (Yousef, El Hendy, El-Demerdash, & Elagamy, 2002). Studies have showed that zinc exhibits a variety of bioactive activities (e.g. antioxidant, anticancer and immunity-enhancing effects) *via* direct and indirect mechanisms (Hammermueller, Bray, & Bettger, 1987). However, zinc deficiency is prevalent worldwide according to the World Health Organization (Prasad, 2013).

Three types of zinc supplements are available on the market: 1) inorganic zinc salts (e.g. zinc sulfate and zinc nitrate), with extremely low bioavailability and severe side effects on the gastrointestinal tract; 2) improved inorganic zinc salts (zinc gluconate and zinc citrate), with improved bioavailability and decreased severe side effects, but still affecting gastrointestinal digestion; 3) biological zinc, with significant bioavailability and no toxicity and hazards, including polysaccharide chelated zinc, protein chelated zinc, polypeptide chelated zinc (Caetano-Silva, Netto, Bertoldo-Pacheco, Alegría, & Cilla, 2021). Compared with inorganic zinc, many natural substances may have the potential to be used (Zhong, Farag, Chen, He, & Xiao, 2022), natural polysaccharide-zinc complex has significant advantages as a biological zinc supplement. Prepared *Athelia rolfsii* exopolysaccharide-zinc complexes were more effective than inorganic and organic zinc supplements in treating zinc deficiency and improving antioxidant activities *in vivo* (Dong, Li, & Min, 2018). Furthermore, *Dictyophora indusiata* polysaccharide–zinc complexes were reported to have a significant anti-proliferative activity against a group of human cancer cell lines *via* activation of caspases-3, −8, and −9, mitochondrial dysfunction, and overproduction of reactive oxygen species (ROS) (Liao, Lu, Fu, Ning, Yang, & Ren, 2015), this kind of biological activity is irreplaceable by inorganic zinc and organic zinc. Zhang et al. (2022) studied a seaweed polysaccharide-zinc complex, and after animal experiments found that modulating mucosal structure improved the intestinal physical barrier function and alleviated intestinal inflammation by inhibiting the TLR4/NF-κB signaling pathway. Zhang et al. (2020) synthesized the rattan polysaccharide zinc inclusion complex for the first time, and tested its antidiabetic activity on streptozotocin-induced diabetic rats. Pharmacological studies showed that *T*-CHO, TG and LDL-C levels decreased substantially, while HDL-C levels increased

* Corresponding authors.
E-mail addresses: xxalxm@126.com (X. Lu), xgqiao@sdau.edu.cn (X. Qiao).

https://doi.org/10.1016/j.fochx.2022.100361
Received 25 January 2022; Received in revised form 5 June 2022; Accepted 9 June 2022
Available online 14 June 2022

with complex treatment. The rattan polysaccharide zinc inclusion complex can be considered as a potential candidate for developing a functional food ingredient of zinc supplement with hypoglycemic effect.

Garlic polysaccharides (GPs) are a widely recognized prebiotic and have a (2 → 1)-linked β-D-Fruf backbone and (2 → 6)-linked β-D-Fruf branched chains (Qiu, Zheng, Zhang, Sun-Waterhouse, & Qiao, 2020). However, there are few reports on the chelation of GPs and zinc ions to improve the bioavailability and health effect of zinc. Considering that GPs have several biological activities (immune-enhancing, antiviral, antioxidant, mineral absorption-promoting, intestinal flora-regulating and liver-protecting effects). Therefore, we hypothesized that the synergy of GPs and Zn could improve the absorption of Zn while producing other good biological effects on the body.

In this paper, the preparation process of GP-Zn (II) complexes was optimized based on response surface methodology. The resulting complexes were structurally characterized based on a series of spectroscopic and chromatographic techniques. After *in vitro* simulated gastrointestinal digestion was analyzed, their bioactivities as a zinc supplement in Zn-deficient mice was evaluated based on health status, enzyme activity and colonic morphology. The results are expected to indicate the high potential of these complexes in food and pharmacological applications.

2. Materials and methods

2.1. Materials and chemicals

Fresh garlic was purchased from Laiwu (Shandong, China) and stored at −2 ± 0.5 °C. The Zn-deficient feed was obtained from Xiaoshuyoutai Biotechnology Co., Ltd. (Beijing, China), and its composition was shown in Table S1. NO content determination kit, mouse ALP ELISA kit, malondialdehyde (MDA) content determination kit, mouse super oxidase dismutase (SOD) ELISA kit and zinc ion determination kit were provided by Shanghai Enzyme-linked Biotechnology Co., Ltd. (Shanghai, China). Zinc gluconate tablets (14.23 mg Zn/100 mg Table) were purchased from Hainan Pharmaceutical Factory Co., Ltd. (Hainan, China). All other chemicals were of analytical grade.

2.2. Extraction and purification of GPs

As described by Li et al. (2021) GPs were isolated from fresh garlic bulb *via* hot water extraction method at 60 °C for 180 min at a ratio of 1:10 (*w/v*). The obtained crude polysaccharides were purified by Sevag reagent (chloroform: butyl alcohol = 4:1, *v/v*), precipitated by 4-fold volume of absolute ethanol, and then freeze-dried for subsequent experiments.

2.3. Preparation of GP-Zn (II) complexes

2.3.1. Synthesis of GP-Zn (II) complexes

$ZnSO_4{\cdot}7H_2O$ was dissolved in distilled water to obtain zinc sulfate concentrate (20 g/L) and diluted to different concentrations (0.02–2 g/L). Then, the $ZnSO_4$ solution was mixed with GP solution (2 g/L) at a ratio of 1:1 (*w/w*) using a vortex mixer, and the pH was adjusted to 3.0–8.0 using HCl solution or NaOH solution (0.5 mol/L). After reaction at 40–80 °C and 150 r/min for 30–150 min, 4-fold volume of absolute ethanol was added and left at 4 °C for 12 h. The obtained GP-Zn (II) complexes were washed with ethanol and freeze dried for further study. According to the content of zinc (II) in the supernatant measured by flame atomic absorption spectrophotometer, the chelation rate of GP-Zn (II) complexes was calculated as follows:

$$\text{Chelation rate}\ (\%) = \frac{Initial\ Zn\ content\ (mg/L) - Non - chelated\ Zn\ content\ (mg/L)}{Initial\ Zn\ content\ (mg/L)} \times 100\%$$

2.3.2. Single-factor experiment

The effect of chelation time, pH, temperature and mass ratio of GPs to $ZnSO_4$ on the chelation rate were investigated by single-factor experiments. First, 3 mL of GP solution was reacted with 3 mL of $ZnSO_4$ solution with the final mass ratios of 1:1, 1:0.5, 1:0.4, 1:0.3, 1:0.2, 1:0.1, 1:0.05, 1:0.01 to obtain the optimal ratio. Then, GP-Zn (II) complexed (mass ratio of GPs to Zn (II) of 1:0.25) was prepared at different temperatures (40, 50, 60, 70 and 80 °C) to analyze their effects on the preparation of complexes. Finally, the response of the chelation rate to the other factors was evaluated by changing the pH (3, 4, 5, 6, 7 and 8) and the reaction time (30, 60, 90, 120 and 150 min).

2.3.3. Response surface experimental design

As presented in Table S4, a Box-Behnken response surface design with four independent variables (A, chelation time; B, pH; C, temperature; D, mass ratio of GPs to $ZnSO_4$) at three levels was performed based on the results of the single-factor tests. According to visualized surfaces and contour plots, statistical models and optimal points were obtained using the chelation rate of GP-Zn (II) complexes as the response. All described experiments were performed in triplicate, independently.

2.4. Chemical composition of GP-Zn (II) complexes

The total sugar content of GPs and their zinc complexes was determined by phenol-sulfuric acid method, with glucose as a standard. The protein content was analyzed by the Bradford method. The uronic acid was quantified by the m-hydroxybiphenyl colorimetric method, as glucuronic acid as a standard (Han et al., 2016).

2.5. Scanning electron microscope (SEM) analysis

The micro-morphological features of GPs and GP-Zn (II) complexes were observed by SEM. The powders of GPs and GP-Zn (II) complex were deposited directly on the specimen stub and sprayed with a thin gold layer. Under high vacuum conditions, their images were acquired at magnifications of 500× and 20000× and at a voltage of 5 kV.

2.6. Structural characterization of GP-Zn (II) complexes

2.6.1. Molecular weight analysis

The molecular weights of GPs and GP-Zn (II) complexes were determined by high performance liquid chromatography coupled with a refractive index detector (HPLC-RID). The GPs and their zinc complexes were prepared as 5 mg/mL solutions and purified by 0.22 μm filters. Then, 20 μL of sample was injected into tandem chromatography columns (Shodex OHpak SB-803HQ, Shodex OHpak SB-802.5HQ, Shodex OHpak SB-802HQ; 300×38 mm, 6 μm) and analyzed at 30 °C, with 0.3 mol/L $NaNO_3$ as the mobile phase at a flow rate of 0.3 mL/min (Li et al., 2021).

2.6.2. Monosaccharide composition analysis

According to the method of Yang, Rainville, Liu, and Pointer (2021a), high performance anion exchange chromatography coupled with a pulsed amperometric detector (HPAEC-PAD, Thermo Fisher ICS-5000, USA) was used to measure the monosaccharide composition of GPs and their zinc complexes. Briefly, 10 mg polysaccharide powder was hydrolyzed with 2 mL of 2.0 mol/L trifluoroacetic acid (TFA) at 80 °C for 4 h, and then treated with nitrogen flushing to remove the residual TFA. After the hydrolyzed samples were purified by Supelclean™ ENVI-18 SPE tubes (500 mg/6 mL) (Supelco, USA) and 0.22 μm millipore

filters, the analysis was conducted using Dionex™ AminoPac™ PA10 IC column (Dionex, 3×250 mm) at 30 °C. The flow rate of 0.20 mol/L NaOH solution and 1.0 mol/L NaAC solution was set as 0.25 mL/min.

2.6.3. Ultraviolet (UV) spectroscopy analysis

The UV spectra of GPs and GP-Zn (II) complexes (2 mg/mL) were acquired from 190 nm to 800 nm using an UV-2450 spectrophotometer (Shimadzu, Japan) at room temperature (Mitić et al., 2011).

2.6.4. Fourier transform infrared (FTIR) spectroscopy analysis

The structural information of GPs and GP-Zn (II) complexes was recorded using a Thermo Nicolet IS10 FTIR spectrometer equipped with a universal ATR accessory (Thermo Fisher Scientific Inc., USA). Two powder samples (3 mg) were placed directly on a conic accessory plate and then scanned 64 times in the wavenumber range of 4000 to 400 cm^{-1} at a resolution of 4 cm^{-1}, in triplicate. After background spectra of air was scanned, the results were analyzed using OMNIC 8.2.0.387 software (Fauziee, Chang, Mustapha, Nor, & Lim, 2021; Yu et al., 2022).

2.6.5. X-ray diffraction (XRD) analysis

The XRD patterns of GPs and GP-Zn (II) complexes were analyzed by an EMPYREAN X-ray diffractometer (Panalytical B.V., Netherlands). The data were produced in the diffraction angle (2θ) range of 5°–80° at 25 °C with a step rate of 1°/min (Ji, Hou, Yan, Shi, & Liu, 2020).

2.6.6. Circular dichroism (CD) spectroscopy analysis

Chirascan ACD (Applied Photophysics, UK) was used to produce CD spectra of polysaccharide samples in the range of 180–450 nm. The sampling time of a single data point was 0.5 s and the bandwidth was 1 nm.

2.6.7. Thermal analyses

The thermodynamic behaviors of GPs and GP-Zn (II) complexes were evaluated by an STA 6000 simultaneous thermal analyzer (PerkinElmer, Waltham, Massachusetts, USA). Two polysaccharide samples were transferred to a standard aluminum pan and hermetically sealed, followed by heating from 30 °C to 600 °C at a rate of 10 °C/min. The nitrogen gas was provided at a flow rate of 20 mL/min.

2.6.8. Particle size, polymer dispersity index (PDI) and zeta potential

The Malvern NANO-Z Zetasizer (Malvern Instruments Limited, Malvern, UK) was used to evaluate the particle size, PDI and zeta potential of GPs and GP-Zn (II). The polysaccharide samples were prepared as solutions and then determined at 25 °C (Abodinar, Smith, & Morris, 2014).

2.7. In vitro simulated gastrointestinal digestion of GP-Zn (II) complexes

As described by Yang et al. (2021b), GP-Zn (II) complexes were subjected to simulated gastrointestinal digestion, with slight modifications. First, the polysaccharide solutions were mixed with the same volume of artificial saliva, followed by incubation at 37 °C for 3 min. The obtained mixture was sampled for zinc ion assay. Then, the residual samples were treated with artificial simulated gastric juice at 37 °C for 5 h. An aliquot of 5 mL sample was taken every 30 min for compositional analysis. Finally, the oral and gastric digestion samples were incubated with artificial simulated intestinal fluid at 37 °C for 3 h. During the simulated digestion, 5 mL of the mixture was sampled for the determination of dissolution rate of Zn (II).

2.8. Effect of GP-Zn (II) complexes on Zn-deficient mice

All animal experiments were approved by Institutional Animal Care and Use Committee of Shangdong Agricultural University (Approval No2021-04). SPF-grade male Kunming mice (11 ± 0.2 g, 3-week-old) were obtained from Jinan Pengyue Laboratory Animal Breeding Co., Ltd. (Shandong, China). All mice were housed in cages (cleaned with EDTA solution) of standard animal laboratory with a relative humidity of 60 ± 5% and a temperature of 23 ± 1 °C, and received their assigned diet and water ad libitum. After 7 days of acclimatization feeding, mice were randomly divided into seven groups: normal control group (fed with a normal mouse diet), model group (fed with a Zn-deficient diet) and five treatment groups (fed with a Zn-deficient diet supplemented daily by gavage with GPs [128.19 mg/kg body weight], $Zn(SO)_4$ [6.96 mg Zn/kg body weight], Zinc gluconate [6.96 mg Zn/kg body weight], GP-Zn (II) complexes at a low dose [3.48 mg Zn/kg body weight], GP-Zn (II) complexes at a high dose [6.96 mg Zn/kg body weight]). The zinc dose for each experimental group is shown in Table S5. During three weeks of the experiment, these mice were provided with deionized water and observed daily for body weight, food intake and health status (Huang et al., 2020). At the end of the experiment, mice in each group were fasted for 12 h and anesthetized with pentobarbital sodium (50 mg/kg) by intraperitoneal injection. The blood was collected from the eyeballs and centrifuged at 2000 rpm/min for 10 min at 4 °C to obtain serum. The serum was stored at −80 ℃. Zn content, MDA content, NO content, ALP activity and SOD activity within the serum were determined using a commercially available detection kit.

Finally, mice were sacrificed by cervical dislocation. The liver, renal, spleen and testis were removed and washed repeatedly with normal saline. After the excess water was dried with absorbent paper, the organ wet weight was obtained. Sections of colon and testis tissue were fixed overnight in 4% paraformaldehyde and subjected to pathological analysis by Hematoxylin Eosin (H&E) staining. In addition, other liver and kidney tissues were homogenized (1:9, w/v) with normal saline (0.9%, w/v) and centrifuged (6000 g, 4 °C, 15 min), and the supernatant was used for the determination of Zn content, MDA content, NO content, ALP activity and SOD activity.

2.9. Statistical analysis

All experimental results were determined in triplicate and expressed as mean ± standard deviation (SD). One-way ANOVA was used for statistical analysis using SPSS statistical software at $P < 0.05$.

3. Results and discussion

3.1. Preparation of GP-Zn (II) complexes

3.1.1. Effect of different factors on the chelation rate of GP-Zn (II) complexes

As shown in Fig. S1A, the ratio effects of GPs to Zn(II) (1:0.4, 1:25, 1:0.2, 1:0.1, 1:0.05 g/g) on the zinc content of GP-Zn (II) complex were researched, as well as fixing other factors (extraction time 120 min, extraction temperature 50 °C and pH 6). As the mass ratio of garlic polysaccharides to Zn^{2+} decreased, the chelation rate showed a trend of increasing first and then decreasing. The maximum chelation rate was achieved (89.4%) at the mass ratio of garlic polysaccharides to Zn^{2+} of 1:0.2. Further increase in the mass ratio would lead to a decrease in the chelation rate. This might be due to the fact that the binding of a hydroxyl group on polysaccharides with Zn^{2+} was bounded in the higher viscosity system (Demchenko, Rusyn, & Saburova, 1989).

It can be seen from Fig. S1B when the temperature of the system gradually increased from 30 °C to 70 °C, the chelating effect of garlic polysaccharide on zinc gradually increased and reached the maximum value (83.4%) at 50 °C. However, after 50 °C, with the increase of temperature, the chelating rate of garlic polysaccharide decreased, dropping to 80.63% at 70 °C. It is speculated that the rising stage may be due to the continuous loosening of the broken groups of garlic polysaccharides, which may collide and combine with the free Zn^{2+} in the system. In the descending stage, the free ions in the system vibrate violently with the rapid increase of temperature, and zinc ions at the original binding site fall back into the free system(Treanor, Rich, & Rehm, 1968).

The chelation rate of the GP-Zn (II) complexes reached the highest level (87.94%) at pH 6.0 (Fig. S1C). The strongly acidic conditions were not favorable for both the binding of zinc ions to –OH on polysaccharide chains and the stabilization of the GP structure ((2 → 1)-linked β-D-Fruf backbones alone or linked by the (2 → 6)-linked β-D-Fruf branched chains). It may also be related to the autocatalytic reaction of polysaccharides in weak acidic environments to obtain more hydroxyl groups (Chan et al., 2011). Although the chelation rate increased with increasing pH of the system under alkaline conditions, this might be due to the formation of $Zn(OH)_2$ precipitations (Morcali, 2015). Therefore, 6.0 was considered to be the optimal pH.

Fig. S1D shows that chelation time also affects the chelation rate. With the extension of time, reaching As time goes by, the chelation rate is increasing, and the chelation rate reaches 87.27% at 120 min. However, after 120 min, the chelation rate did not increase with the extension of time but showed a trend of slow decline. Because the combination of garlic polysaccharide and Zn^{2+} was unstable and uneven in a short time, however, too long time will produce other unnecessary by-products, so the chelation rate slowly decreases (87.27%-84.72%).

3.1.2. Optimization of synthesis conditions for GP-Zn (II) complexes

Table S6 showed the Box-Behnken design matrix and its response values for the chelation rate of GP-Zn (II) complexes. A total of twenty-nine independent variable combinations was produced, with chelation rates ranging from 66.42% to 90.11%. According to the multiple regression analysis of the experimental results, the fitted polynomial equation was obtained as follows:

$$Y = 84.32 - -1.10A - 1461B - 4.66C + 0.99D + 0.60AB - 4.57AC + 0.45AD + 2.29BC - 0.50BD + 3.39CD - 2.65A^2 - 9.72B^2 - 10.19C^2 - 0.35D^2.$$

From the regression coefficients, the quadratic effects of three factors (pH, temperature and mass ratio) were highly significant ($P < 0.01$), while the coefficient of quadratic effect of time to the chelation rate of GP-Zn (II) complexes was significant ($P < 0.05$). Meanwhile, the primary term (temperature) and interaction terms (pH and mass ratio) on the chelation rate was highly significant ($P < 0.01$), and the primary term (pH and mass ratio) and interaction terms (temperature and mass ratio, mass ratio and time) were significant ($P < 0.05$). As shown in Table S7, the P value of the model was < 0.001 and the fitting value was >0.05, indicating that the predictive quadratic regression model could sufficiently represent the actual chelation rate of GP-Zn (II) complexes, which could be used to optimize the preparation conditions of GP-Zn (II) complexes.

Three-dimensional response surface plots and contour plots could directly reflect the effects and interactions of the four factors on the chelation rate of GPs-Zn (II) complexes. As shown in Fig. S2A, the steep response surface and dense contour lines suggested that the effect of temperature on the synthesis of GP-Zn (II) complexes was the most significant, and the response of the chelation rate to mass ratio and pH was more pronounced than that of the time. Furthermore, there were significant interactions between pH and mass ratio on the GP-Zn (II) complexes (elliptical contour lines), followed by mass ratio with temperature and time. However, no obvious interactions were present in pH and temperature, pH and time, temperature and time. Based on the response surface analysis, the optimal preparation conditions for GP-Zn (II) complexes were as follows: mass ratio of GPs to Zn^{2+} of 1:0.21, temperature 53 °C, pH 5.9 and time 119.75 min, with the maximum chelation rate of 90.11%. The verification tests showed that the actual chelation rate was 90% under the optimal synthesis conditions, with no significant difference between the predicted value and the experimental value at a 5% level of significance. Therefore, the proposed model and equations were accurate and reproducible, which could guide the processing of GP-Zn (II) complexes.

3.2. Physicochemical property

The total sugar content of GPs and their zinc complexes was 91.23% and 89.41%, respectively. The protein content and uronic acid content of GPs were 2.30% and 3.75%, respectively, which were 1.69% and 1.37% for GP-Zn (II) complexes. According to inductively coupled plasma mass spectrometry, GP-Zn (II) complexes contained 5.15% Zn (II).

3.3. Morphological characteristics

Fig. 1 showed the surface morphological images of GPs and GP-Zn (II) complexes. After freeze-drying, GPs were light yellow powder, while GP-Zn (II) complexes were white powder. They both had no specific irritating odor. SEM images with different magnifications provided micro-morphological characteristics of the dried polysaccharide samples (Kacurakova, Capek, Sasinkova, Wellner, & Ebringerova, 2000). Both polysaccharide polymers were composed of thin sheets with relatively flat surfaces, but the GP-Zn (II) complexes looked more complete and rough. Under higher magnification (10,000×), some irregular protrusions appeared on the surface of GP-Zn (II) complexes. In contrast, the surface of GPs was relatively flat. The difference of surface morphology might be partly due to the structural characteristics.

3.4. Structural characterization

3.4.1. Monosaccharide composition and molecular weight analyses

Table 1 summarized the monosaccharide composition and molecular weights of GPs and their zinc complexes. Fructose and glucose were the dominant monosaccharides in two polysaccharide polymers. Although arabinose and galactose were also detected, they had low abundance (<2.0 %) and might be derived from residual traces of pectin. Two polysaccharide samples differed in mass ratios, where GP-Zn (II) complexes had a higher proportion of fructose. Furthermore, the Mw of GPs increased from 3684 Da to 6448 Da after chelation with Zn (II). However, the polydispersity index (Mw/Mn) value decreased from 2.12 to 1.53. Therefore, GP-Zn (II) complexes had higher Mw and more concentrated distribution, which might be due to the binding of some polysaccharides after the chelation with Zn (II).

3.4.2. Particle size, PDI and zeta potential

As shown in Table 1, GP-Zn (II) complexes had a larger particle size and more concentrated distribution compared with GPs. Furthermore, the zeta potential of GP-Zn (II) complexes was decreased greatly from −1.81 mV to −9.30 mV. This might be due to the fact that the binding of GPs and Zn caused a greater electrostatic repulsion between the particles and led to a stronger dispersion than aggregation, which made the GP-Zn (II) complex solution more stable (Griesser et al., 2017; Subasi, Xiao, & Capanogluo, 2021).

3.4.3. UV and FTIR spectral analyses

Fig. 2A showed that there were no obvious absorption peaks between 260 nm and 280 nm. Combined with the results of the physicochemical indicators, two polysaccharide samples contained little protein. FTIR spectra could reflect the structural characteristics of both polysaccharide samples (Zhu, Li, Ma, Xu, Zhou, Jia, Zha, Xue, Tao, Xiong, Yuan, & Chen, 2020). As shown in Fig. 2B, GPs and GP-Zn (II) complexes had typical IR bands of polysaccharides: 3300–3200 cm^{-1} (O—H stretching vibrations of hydroxyl groups), 2930 cm^{-1} (C—H stretching vibrations), 1590 cm^{-1} (anti-symmetrical C═O stretching vibrations of ionic carboxyl groups) and 1400 cm^{-1} (symmetrical C═O stretching vibrations of ionic carboxyl groups), 1200–800 cm^{-1} (O—C—O and C—O—C stretching vibrations of glycosidic linkages and rings or C—O—H stretching vibrations). However, some slight changes were observed after chelation of GPs and Zn (II). For example, the bands representing O—H stretching vibrations of hydroxyl groups shifted from 3257 cm^{-1} for GPs to 3290

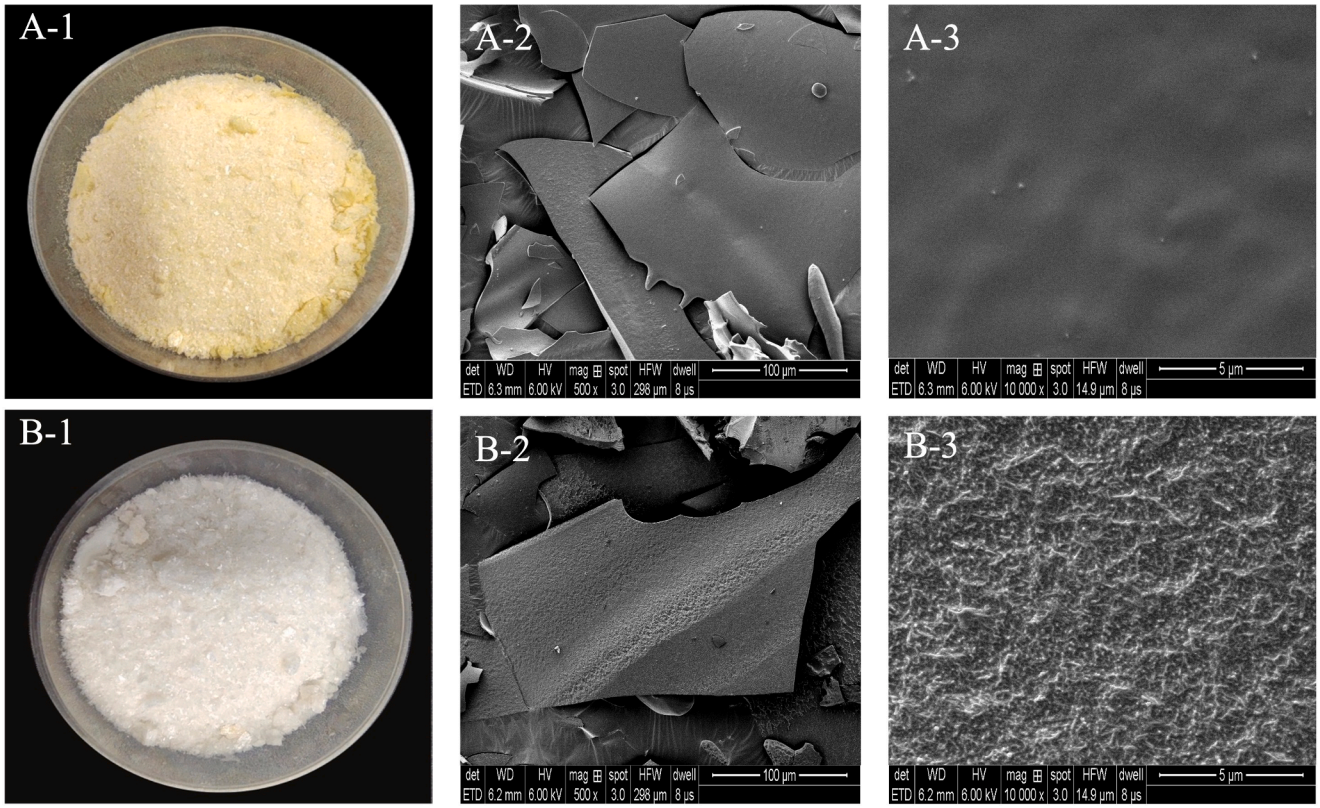

Fig. 1. Surface morphological images of garlic polysaccharides (A) and their zinc complexes (B).

Table 1
Monosaccharide composition and molecular weight of garlic polysaccharides (GPs) and GP-Zn(II) complexes and their particle size, PDI and Zeta potential.

	GPs	GP-Zn (II) complexes
Monosaccharide composition		
Fucose (%)	–	–
Rhamnose (%)	–	–
Arabinose (%)	1.003	1.23
Galactose (%)	0.358	0.845
Glucose (%)	16.84	10.08
Mannose (%)	–	–
Xylose (%)	–	–
Fructose (%)	82.76	89.35
Galacturonic acid (%)	–	–
Glucuronic acid (%)	–	–
Molecular weight		
Mn (Da)	1737	4205
Mw (Da)	3684	6448
Mz (Da)	6415	8794
Mw/Mn (Da)	2.12	1.53
Particle size (nm)	86.93 ± 3.55	94.18 ± 2.88
PDI	0.363 ± 0.0235	0.304 ± 0.0359
Zeta potential (mV)	−1.81 ± 0.79	−9.30 ± 1.72

cm^{-1} for GP-Zn (II) complexes, accompanied by a slight decrease in the intensity of this signal. This indicated that the chelation of polysaccharides and Zn (II) might occur at the hydroxyl groups. Furthermore, the obvious change in the number and signal intensity in the range of 1200–800 cm^{-1} suggested that the chelation of polysaccharides and Zn (II) affected the O—C—O/O—C—O stretching vibrations (Yan et al., 2021).

3.4.4. XRD analysis

Fig. 2C showed the XRD patterns of GPs and GP-Zn (II) complexes. The wide diffraction peak at 2θ 22.34° indicated the semi-crystalline nature of GPs, which was similar to that of *Ganoderma lucidum* polysaccharides (Li et al., 2019). After chelation with Zn (II), the intensity of this diffraction peak was increased significantly, and three sharp peaks (which were weak in GPs) became very obvious. Therefore, the formation of GP-Zn (II) complexes altered the original structure of the polysaccharides, and their significantly enhanced crystallinity might be due to the non-covalent interactions of the hydroxyl groups of GPs and Zn (II).

3.4.5. CD analysis

CD spectra could be used to study the structure of sugars (Johnson, 1987). It could be seen from Fig. 2D that the absorption peaks of GPs and GP-Zn(II) complexes appeared after 190 nm, indicating the typical characteristics of sugars. The changes in ellipticity can be used to distinguish the complex equilibrium of individual asymmetric monosaccharides freely taken in solution, the ovality of the two after 246 nm fluctuates up and down the X axis, indicating that neither has a spiral structure (Johnson, 1987). Compared with GPs, the absorption peaks of the zinc complexes of GPs were significantly shifted, indicating the changes in chemical bonding.

3.4.6. TG and DTG analysis

The stability of drugs, especially thermal stability, is one of the most important indicators for the development of health care products and drugs (Gao, Zhu, Liu, Cui, & Abd El-Aty, 2021). The DTG curves reveal the temperatures exhibited by GPs and GP-Zn(II) at the maximum mass loss rate, and the TG curves show the changes in the percentage of mass loss of GPs and GP-Zn(II) over the decomposition temperature range (Chang, Yu, Ma, & Anderson, 2011). As presented in Fig. 2E and Fig. 2F, thermodynamic behavior of GPs and GP-Zn (II) complexes showed greater similarities and smaller differences. In TG profiles, the thermal decomposition of two polysaccharide samples contained two stages: the loss of moisture and volatiles in the range of 28–150 °C (GP-Zn (II)

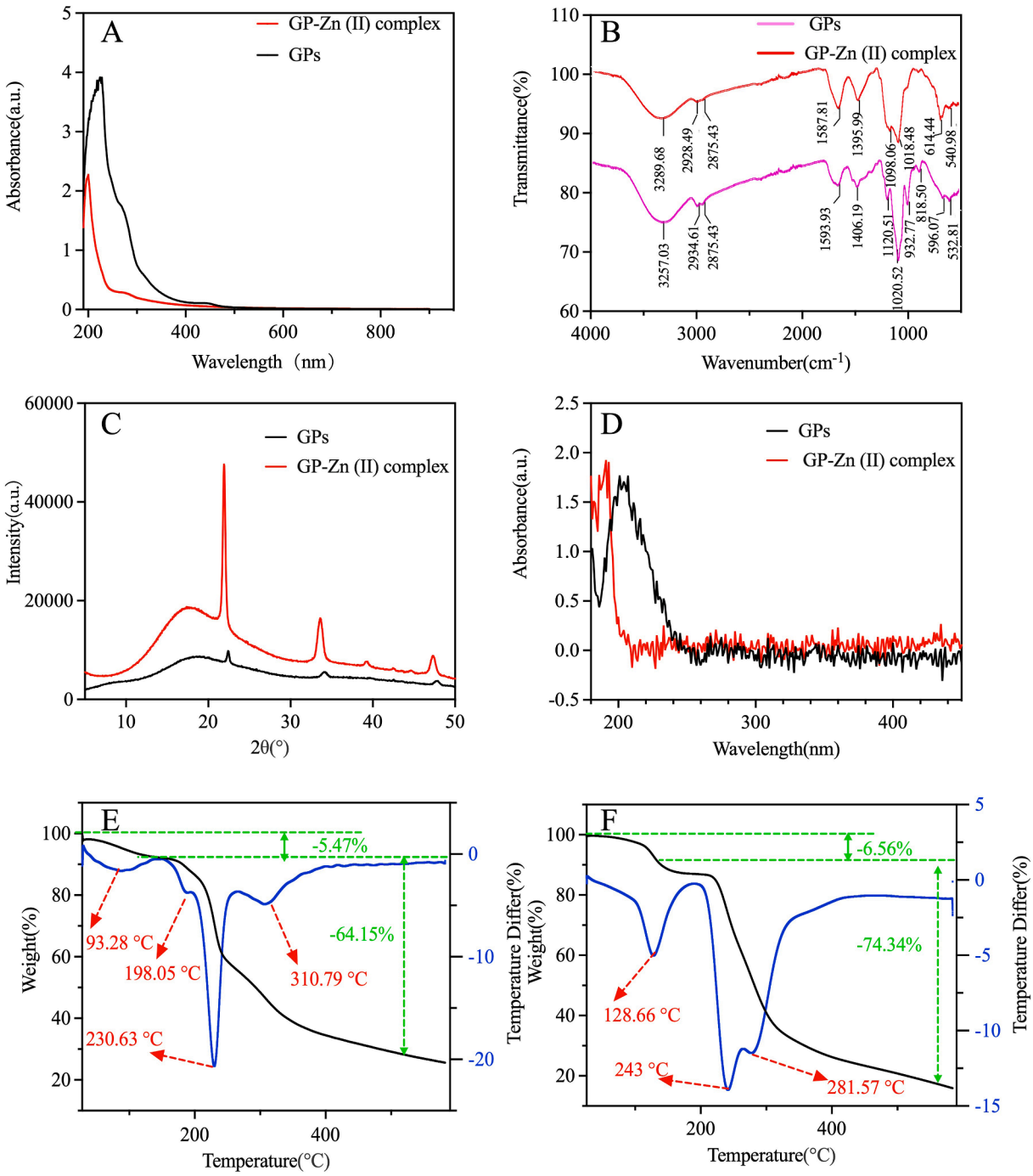

Fig. 2. UV (A) and FTIR (B) spectra of garlic polysaccharides and garlic polysaccharide-Zn (II) complexes;X-ray diffraction pattern (C) and CD analysis (D) of garlic polysaccharides and garlic polysaccharide-Zn (II) complexes; thermodynamic analysis of garlic polysaccharides(E) and garlic polysaccharide-Zn (II) complexes (F).

complexes had a higher rate of mass loss than GPs), and decarboxylation and thermal decomposition of the polysaccharide structure (64.15% and 74.34% for GPs and GP-Zn (II) complexes, respectively) (Mothé & de Freitas, 2013). In DTG curves, there were great differences between GPs and GP-Zn (II) complexes. The first endothermic peak was 128.66 °C for GP-Zn (II) complexes, which was significantly higher than that of GPs. Furthermore, the maximum decomposition rates appeared at 243.0 °C and 281.57 °C for GP-Zn (II) complexes, while was only 230.63 °C for GPs. According to the above results, the modification of Zn (II) could significantly enhance the thermal stability of GPs. This is related to the increase in the crystallinity of GP-Zn obtained from X-diffraction analysis (D'Amico, Manfredi, & Cyras, 2012).

3.5. *In vitro simulated gastrointestinal digestion of GP-Zn (II) complexes*

In this experiment, the zinc release of GP-Zn (II) complexes, zinc gluconate and $ZnSO_4$ during simulated gastrointestinal digestion was analyzed by simulated saliva, gastric fluid and intestinal fluid. As shown in Fig. S3, the Zn(II) release rates of GP-Zn(II) complexes (0.148%), zinc gluconate (2.141%) and ZnSO4 (2.035%) in simulated saliva digestion for 30 min, indicating that all of three zinc supplements are very stable in saliva. In the process of simulating digestion of gastric juice, zinc gluconate compared with GPs-Zn(II) complex, zinc (II) release rate is higher, gastric juice after 4 h zinc release rate reached 38.746%. The zinc release rate of $ZnSO_4$ was 52.509% in the stomach for 0.5 h, and the

zinc release rate in the simulated gastric juice and intestinal fluid after that was almost unchanged. The highest Zn(II) release rates of GP-Zn(II) complex (23.09%) and zinc gluconate (45.97%) occurred in the simulated intestinal fluid. GP-Zn(II) enters the intestine more stably, achieving the purpose of sustained-release zinc. GP-Zn(II) may release Zn(II) due to degradation of oligosaccharides by gut microbes when entering the body (Rossi et al., 2005).

In simulated intestinal fluid, a slight decrease in the rate of GP-Zn(II) release of complexes and zinc gluconate may be due to the absorption of complex components in the digestive juice, such as proteases, free peptides or esters. During the assay, they are removed by alcohol precipitation. *In vivo* ingestion, Zn (II) could be absorbed in a variety of ways, with free diffusion through the small intestine wall being the most important (Maares & Haase, 2020). Therefore, the dissociated free zinc ions would diffuse rapidly into the small intestinal cells once they were released from GP-Zn (II) complexes and zinc gluconate. Some of the released Zn (II) was also be absorbed by the intestinal wall along with small peptides.

3.6. Effect of GP-Zn (II) complexes on the health of Zn-deficient mice

3.6.1. Effect of GP-Zn (II) complexes on body weight and organ index

After a period of dietary intervention, mice in the Zn-deficient group had a dull coat color, accompanied by hair loss, fur clutter, soiling and bleeding between the toes. Furthermore, mental fatigue and persistent fogging were observed for most of the Zn-deficient mice. However, supplementation of GP-Zn (II) complexes and zinc gluconate alleviated these symptoms caused by zinc deficiency, and improved the coat condition (shiny, intact and clean) and mental status (lively) of mice. As shown in Table 2, the body weight of the mice in the normal group increased significantly from 11.11 g to 28.26 g ($P < 0.05$), but almost no changes were found for Zn-deficient mice after 21 d of feeding ($P > 0.05$). This was due to the fact that zinc deficiency adversely affected the sense of smell and thus the appetite of mice (Shay & Mangian, 2000). Consuming GP-Zn (II) complexes and zinc gluconate led to a significant increase in body weight ($P < 0.05$), and the body weight of mice supplemented with GP-Zn (II) complexes at the high-dose was significantly higher than the other treatment groups, with no significant difference from the normal group ($P < 0.05$). Compared with these two zinc supplements, no significant weight gain was observed in $Zn(SO)_4$-treated group ($P > 0.05$). Dietary zinc had important effects on organ development. The liver, spleen, kidney and testicular indices of mice in the normal group were 45.30, 4.21, 13.19 and 10.27 mg/g, which were significantly reduced to 37.25, 2.10, 12.17 and 8.36 mg/g in the mice of model group ($P < 0.05$). The administration of GP-Zn (II) complexes at the high-dose could significantly increase the liver and testicular indices of mice ($P < 0.05$). Therefore, GP-Zn (II) complexes could be used as a good zinc supplementation to promote the development of these three organs. It was worth noting that the differences were not significant ($P > 0.05$), although the liver and testicular indices of mice treated with GP-Zn (II) complexes at the low-dose were increased. In addition, supplementation of $Zn(SO)_4$ had no effect on organ indices of mice.

Table 2
Body weight changes and organ indices of mice in each group.

Groups	Weight (g)		Organ index (mg/g)			
	Original weight	Final weight	Liver	Spleen	Renal	Testis
Normal group	11.11 ± 0.88	28.46 ± 0.97#	45.30 ± 0.01#	4.21 ± 0.034#	13.19 ± 0.02#	10.27 ± 0.019#
Zinc deficiency group	10.81 ± 0.40	11.02 ± 0.94*	37.25 ± 0.02*	2.10 ± 0.001*	12.17 ± 0.02*	8.36 ± 0.026*
GPs	11.55 ± 0.55	12.04 ± 0.93*	35.93 ± 0.02*,#	1.92 ± 0.002*	11.68 ± 0.03*	8.50 ± 0.017*
$Zn(SO)_4$	11.30 ± 0.73	12.78 ± 0.99*	37.55 ± 0.03*	1.99 ± 0.003*	11.71 ± 0.02*	8.19 ± 0.044*
Zinc gluconate	11.20 ± 0.37	18.43 ± 0.73*,#	37.64 ± 0.02*	1.82 ± 0.002*	12.06 ± 0.02*	9.15 ± 0.028#
GP-Zn (II) complexes at the low-dose	10.95 ± 0.43	18.20 ± 0.83*,#	39.46 ± 0.05	1.89 ± 0.001*	11.33 ± 0.04*	8.90 ± 0.013*
GP-Zn (II) complexes at the high-dose	11.38 ± 0.55	21.50 ± 0.91#	41.96 ± 0.036#	2.11 ± 0.003*	11.34 ± 0.03*	9.36 ± 0.022#

* $P < 0.05$, compared with normal control group.
\# $P < 0.05$, compared with zinc deficiency group.

3.6.2. Effect of GP-Zn (II) complexes on Zn (II) level in mice

As presented in Fig. 3A, zinc levels in serum and liver were lowest in the zinc-deficient group of mice. After the intervention of GP-Zn (II) complexes and zinc gluconate, the levels of zinc in serum and liver were greatly increased, but only the difference in the GP-Zn (II) complex-treated groups was significantly different ($P < 0.05$). Furthermore, supplementation of $Zn(SO)_4$ was only effective for the recovery of zinc contents in the liver ($P < 0.05$), and zinc contents in the serum of the Zn $(SO)_4$-treated group and GP-treated group were basically the same as those of the model group, which was consistent with the previous results (Rojas et al., 1995). Therefore, GP-Zn (II) complexes were effective in improving zinc levels in serum and liver, and its effect was superior to that of the inorganic Zn-treated group.

3.6.3. Effect of GP-Zn (II) complexes on ALP activity

Zinc levels affect the synthesis pathway of ALP *in vivo*, and there is a positive correlation between them (Storrie & Stupp, 2005). Therefore, ALP activity can indirectly reflect the level of zinc in mice and evaluate the effect of zinc supplementation. As presented in Fig. 3B, zinc deficiency resulted in a significant decrease in ALP activity in serum and liver of mice, compared with the control group ($P < 0.05$). However, supplementation of GP-Zn (II) complexes could effectively reverse this damage. In serum, mice in the GP-Zn (II) complex-treated group had the highest ALP activity (0.045–0.048 IU/g), which was significantly higher than that of the model group and $Zn(SO)_4$-treated group. In the liver, the highest ALP activity occurred in the control group (0.056 IU/g), but the intervention of GP-Zn (II) complexes could restore the ALP activity of mice to normal levels (0.046–0.053 IU/g). In contrast, zinc gluconate and zinc sulfate were not sufficient for the supplementation of ALP activity in Zn-deficient mice.

3.6.4. Effect of GP-Zn (II) complexes on NO content, SOD activity and MDA content in serum, liver and kidney

NO has been proven to be an important inflammatory mediator with a potential role in gastrointestinal diseases, and its level is closely related to zinc contents in the body (Xu, Yin, Li, & Liu, 2010). Fig. 3C suggested that the mice in the Zn-deficient group had the highest NO contents in serum (0.49 μmol/L) and liver (48.21 μmol/L). After the administration of GP-Zn (II) complexes at the high-dose, NO levels in serum and liver were significantly reduced by 36.73% and 38.50%, respectively ($P < 0.05$), exhibiting the lowest NO content. Notably, supplementation of GPs and $Zn(SO)_4$ could also significantly alleviate NO levels in serum and liver ($P < 0.05$), but the changes induced by zinc gluconate treatment were not significant ($P > 0.05$).

Zinc levels also affect significantly redox homeostasis, SOD activity and MDA content *in vivo* (Kloubert & Rink, 2015). SOD is one of the major enzymes foe scavenging radicals in the human body, but zinc deficiency could reduce SOD activity and induce cell apoptosis by damaging the steric structure of SOD proteins and catalytic cycling function (Kara et al., 2010). As shown in Fig. 3D, the SOD activity in serum and kidney of mice in the normal group was 2839.06 U/g and

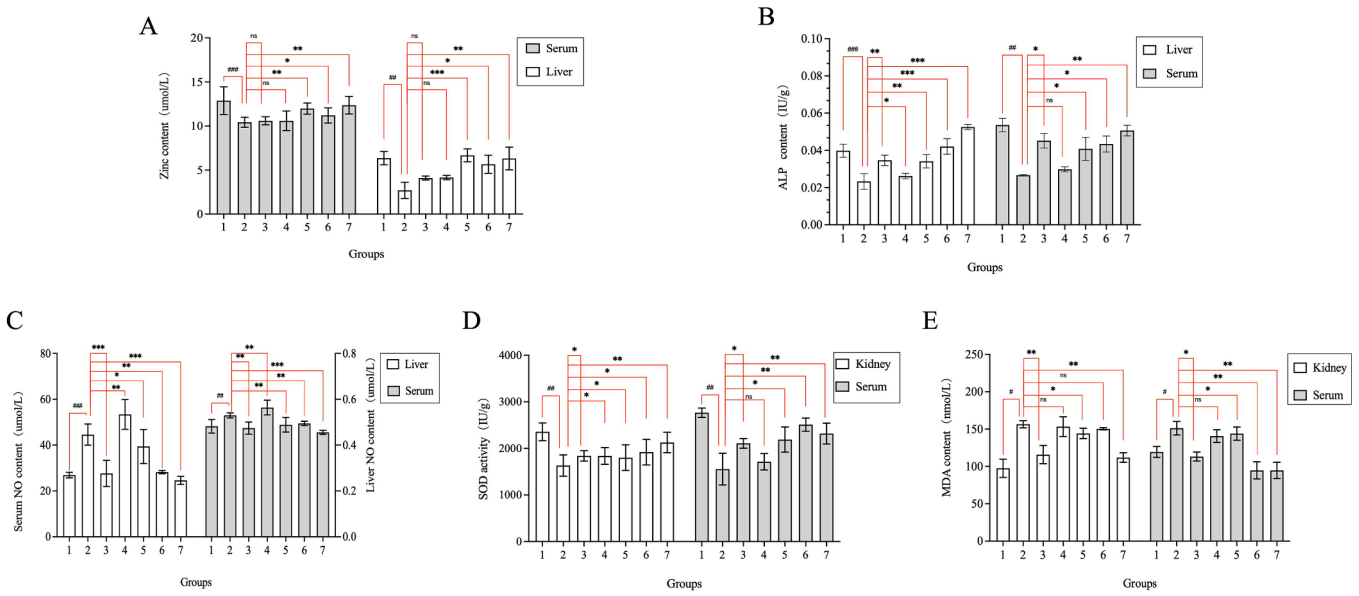

Fig. 3. Zinc content, ALP activity, NO content, SOD activity and MDA content in serum, liver and kidney of mice. 1: Normal group, 2: Zinc deficiency group; 3: GP-treated group; 4: $Zn(SO)_4$-treated group; 5: Zinc gluconate-treated group; 6: GP-Zn (II) complex-treated group at a low dose; 7: GP-Zn (II) complex-treated group at a high dose.

2493.43 U/g, respectively, which was significantly decreased to 1798.71 U/g and 1794.95 U/g due to zinc deficiency ($P < 0.05$). The administration of GP-Zn (II) complexes at the high-dose could significantly increase SOD activity to normal levels ($P < 0.05$). Similar protective effects were observed in serum of mice supplemented with GP-Zn (II) complexes at the high-dose or $Zn(SO)_4$, but the increase in SOD activity in the kidney caused by them was not significant ($P < 0.05$). MDA is a major oxidative stress product. Fig. 3E indicated that Zn-deficient mice had the highest MDA levels (157.58 nmol/L and 159.89 nmol/L in serum and kidney, respectively). However, MDA levels were decreased significantly in serum due to the administration of GP-Zn (II) complexes at the low-dose and high-dose ($P < 0.05$), as well as in kidney due to the treatment of GP-Zn (II) complexes at the high-dose ($P < 0.05$). Notably, supplementation of GPs led to a 25.38% and 22.10% decreases in the MDA contents in serum and kidney ($P < 0.05$), which might be due to the probiotic effect of GPs through the regulation of intestinal flora. This indicated that GP-Zn (II) complexes could play a role as a prebiotic apart from being a good zinc supplement. Accordingly, GP-Zn (II) complexes could effectively alleviate oxidative stress levels by supplementing zinc levels and acting as a prebiotic.

3.6.5. *Effect of GP-Zn (II) complexes on colonic morphology*

Zinc plays an important role in maintaining the integrity of epithelial cells and tissues. In the intestine, zinc promotes the repair of the small intestinal epithelium, and facilitates the reabsorption of sodium and water from the intestinal mucosa (Sunuwar, Medini, Cohen, Sekler, & Hershfinkel, 2016). H&E-staining suggested a small amount of infiltrative changes in the intestinal mucosal barrier and a slight disruption of the intestinal mucosal structure in Zn-deficient mice (Fig. 4A). Although the distribution of intestinal mucosal cells was ordered, some cells were changed. After supplementation of GP-Zn (II) complexes at the high-dose, these damages were effectively alleviated: the intestinal mucosal cells were neatly distributed and their ultrastructure was not altered, with no infiltrative changes. In contrast, the improvement caused by GP-Zn (II) complexes at the low-dose was not significant as in the high-dose group. It was reported that common zinc supplements were irritating to the gastrointestinal tract (Pories, Henzel, Rob, & Strain, 1967). As shown in Fig. 4(A), there was an obvious disruption for mucosal cells and intestinal mucosal ultrastructure when zinc gluconate and $Zn(SO)_4$ were provided, especially in the zinc gluconate-treated group. Therefore, GP-Zn (II) complexes at the low-dose and high-dose could not only

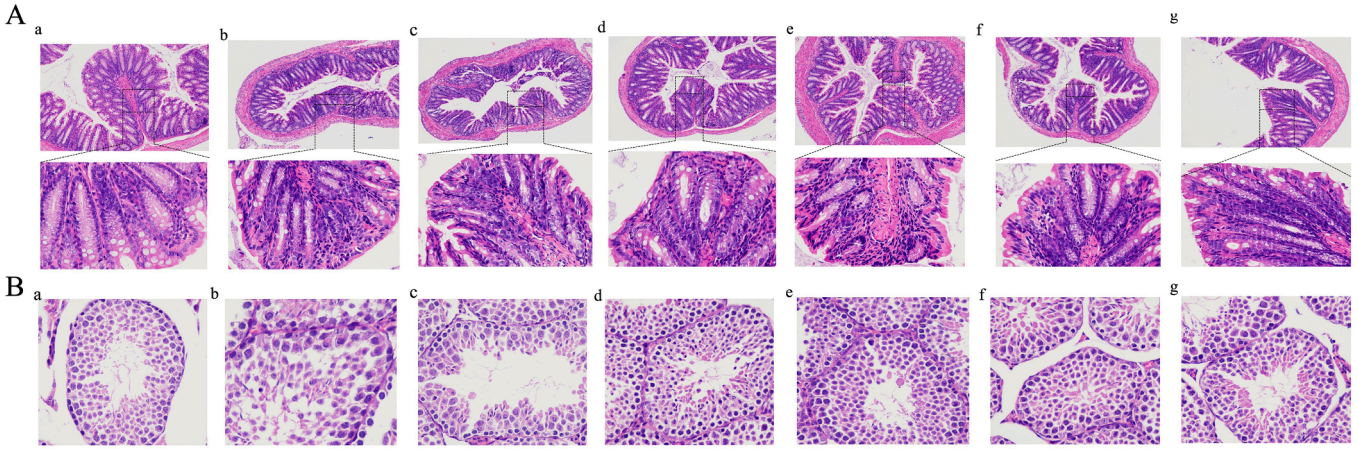

Fig. 4. H&E-stained of the colon(A) and testes(B) in each group. a: Normal control, b: Zinc deficiency group; c: GP-treated group; d: $Zn(SO)_4$-treated group; e: Zinc gluconate-treated group; f: GP-Zn (II) complex-treated group at a low-dose; g; GP-Zn (II) complex-treated group at a high dose.

effectively supplement Zn (II), but also avoid the irritating damage of zinc ions to the intestinal tract.

3.4.6. Effects of GP-Zn (II) complexes on testicular morphology

Zinc plays an extremely important role in the sexual development of the human body, especially in the testes of males and ovaries of females (Prasad et al., 1967). As indicated in Fig. 4(B), the cross-sectional profile of the germinal tubules was uneven and irregular in the testes of mice in the zinc-deficient group, with some structural deformation and inclusions in the germinal epithelium. Although the number of primary and secondary spermatocytes was not observed around the germinal tubules, their number should be reduced and it was difficult to produce spermatocytes and spermatozoa (Hafiez, El-Kirdassy, El-Malkh, & El-Zayat, 1990). After supplementation of GP-Zn (II) complexes and zinc gluconate, the testicles of mice were well developed, with spermatogonial cells near the epithelial lumen of the spermatogonia. Therefore, these two zinc supplements effectively promoted the development of sexual organs in zinc-deficient mice.

4. Conclusions

In this study, the preparation process of GP-Zn (II) complexes was optimized by response surface method, and their effects on the health characteristics of Zn-deficient mice were evaluated after physicochemical and structural characterization was performed. The obtained GP-Zn (II) complexes that were prepared under optimal conditions were composed of fructose and glucose, with an Mw of 6448 Da and Zn (II) content of 5.15%. Structural characterization suggested that the chelation of Zn (II) and GPs likely involved hydroxyl groups and O—C—O structures, and this modification enhanced the crystallinity of GPs and thermal stability. In *intro* simulated gastrointestinal digestion, the GP-Zn (II) complexes meet sustained-release requirements. After 21 days of intervention, GP-Zn (II) complexes could effectively alleviate the damage caused by zinc deficiency, including the increase in body weight and organ indices, Zn (II) level, ALP activity and SOD activity, the decrease in the NO content and MDA content in serum, liver and kidney, as well as mitigation of damage of colonic and testicular tissue. Therefore, GP-Zn (II) complexes had great potential as a good zinc supplement. However, whether it is due to the complete change in the absorption mode of trace elements, such as nanoparticles directly into the blood to be absorbed, or because polysaccharides can play a colon-targeted delivery effect to directly deliver zinc ions into the intestine to be absorbed, it remains to be further discussed and studied.

Declaration of Competing Interest

The authors declare that they have no known competing financial interests or personal relationships that could have appeared to influence the work reported in this paper.

Acknowledgments

This work was supported by the Major Scientific and Technological Innovation Projects of Key R&D Program of Shandong Province (2019JZZY020607); the Special Fund for Leading Talent in Mount Tai of Shandong Province (No.tscy20200121).

Appendix A. Supplementary data

Supplementary data to this article can be found online at https://doi.org/10.1016/j.fochx.2022.100361.

References

Abodinar, A., Smith, A. M., & Morris, G. A. (2014). A novel method to estimate the stiffness of carbohydrate polyelectrolyte polymers based on the ionic strength dependence of zeta potential. *Carbohydrate Polymers, 112*, 6–9. https://doi.org/10.1016/j.carbpol.2014.05.063

Caetano-Silva, M. E., Netto, F. M., Bertoldo-Pacheco, M. T., Alegría, A., & Cilla, A. (2021). Peptide-metal complexes: Obtention and role in increasing bioavailability and decreasing the pro-oxidant effect of minerals. *Critical Reviews in Food Science and Nutrition, 61*(9), 1470–1489. https://doi.org/10.1080/10408398.2020.1761770

Chan, T. H., Chen, P. T., Chang, H. H., Lai, M. Y., Hayashi, M., Wang, J. K., & Wang, Y. L. (2011). Autocatalytic reaction in hydrolysis of difructose anhydride III. *The Journal of Physical Chemistry A, 115*(37), 10309–10314. https://doi.org/10.1021/jp206494r

Chang, P. R., Yu, J., Ma, X., & Anderson, D. P. (2011). Polysaccharides as stabilizers for the synthesis of magnetic nanoparticles. *Carbohydrate polymers, 83*(2), 640–644. https://doi.org/10.1016/j.carbpol.2010.08.027

D'Amico, D. A., Manfredi, L. B., & Cyras, V. P. (2012). Relationship between thermal properties, morphology, and crystallinity of nanocomposites based on polyhydroxybutyrate. *Journal of Applied Polymer Science, 123*(1), 200–208. https://doi.org/10.1002/app.34457

Demchenko, A. P., Rusyn, O. I., & Saburova, E. A. (1989). Kinetics of the lactate dehydrogenase reaction in high-viscosity media. *Biochimica et Biophysica Acta (BBA)-Protein Structure and Molecular Enzymology, 998*(2), 196–203. https://doi.org/10.1016/0167-4838(89)90273-2

Dong, J., Li, H., & Min, W. (2018). Preparation, characterization and bioactivities of Athelia rolfsii exopolysaccharide-zinc complex (AEPS-zinc). *International Journal of Biological Macromolecules, 113*, 20–28. https://doi.org/10.1016/j.ijbiomac.2018.01.223

Fauziee, N. A. M., Chang, L. S., Mustapha, W. A. W., Nor, A. R. M., & Lim, S. J. (2021). Functional polysaccharides of fucoidan, laminaran and alginate from Malaysian brown seaweeds (Sargassum polycystum, Turbinaria ornata and Padina boryana). *International Journal of Biological Macromolecules, 167*, 1135–1145. https://doi.org/10.1016/j.ijbiomac.2020.11.067

Gao, W., Zhu, J., Liu, P., Cui, B., & Abd El-Aty, A. M. (2021). Preparation and characterization of octenyl succinylated starch microgels via a water-in-oil (W/O) inverse microemulsion process for loading and releasing epigallocatechin gallate. *Food Chemistry, 355*, Article 129661. https://doi.org/10.1016/j.foodchem.2021.129661

Griesser, J., Burtscher, S., Köllner, S., Nardin, I., Prüfert, F., & Bernkop-Schnürch, A. (2017). Zeta potential changing self-emulsifying drug delivery systems containing phosphorylated polysaccharides. *European Journal of Pharmaceutics and Biopharmaceutics, 119*, 264–270. https://doi.org/10.1016/j.ejpb.2017.06.025

Hafiez, A. A., El-Kirdassy, Z. H. M., El-Malkh, N. M., & El-Zayat, E. M. I. (1990). Role of zinc in regulating the testicular function part 3. Histopathological changes induced by dietary zinc deficiency in testes of male albino rats. *Food/Nahrung, 34*(1), 65–73. https://doi.org/10.1002/food.19900340114

Hammermueller, J. D., Bray, T. M., & Bettger, W. J. (1987). Effect of zinc and copper deficiency on microsomal NADPH-dependent active oxygen generation in rat lung and liver. *The Journal of Nutrition, 117*(5), 894–901. https://doi.org/10.1093/jn/117.5.894

Han, Q., Wu, Z., Huang, B., Sun, L., Ding, C., Yuan, S., … Yuan, M. (2016). Extraction, antioxidant and antibacterial activities of Broussonetia papyrifera fruits polysaccharides. *International Journal of Biological Macromolecules, 92*, 116–124. https://doi.org/10.1016/j.ijbiomac.2016.06.087

Huang, Q., Teng, H., Chang, M., Wang, Y., He, D., Chen, L., & Song, H. (2020). Mass spectrometry-based metabolomics identifies the effects of dietary oligosaccharide-zinc complex on serum and liver of zinc deficiency mice. *Journal of Functional Foods, 65*, Article 103777. https://doi.org/10.1016/j.jff.2020.103777

Ji, X., Hou, C., Yan, Y., Shi, M., & Liu, Y. (2020). Comparison of structural characterization and antioxidant activity of polysaccharides from jujube (Ziziphus jujuba Mill.) fruit. *International Journal of Biological Macromolecules, 149*, 1008–1018. https://doi.org/10.1016/j.ijbiomac.2020.02.018

Johnson, W. C. (1987). The circular dichroism of carbohydrates. *Advances in Carbohydrate Chemistry and Biochemistry, 45*, 73–124. https://doi.org/10.1016/S0065-2318(08)60137-7

Kacurakova, M., Capek, P., Sasinkova, V., Wellner, N., & Ebringerova, A. (2000). FT-IR study of plant cell wall model compounds: Pectic polysaccharides and hemicelluloses. *Carbohydrate Polymers, 43*(2), 195–203. https://doi.org/10.1016/S0144-8617(00)00151-X

Kara, E., Gunay, M., Cicioglu, İ., Ozal, M., Kilic, M., Mogulkoc, R., & Baltaci, A. K. (2010). Effect of zinc supplementation on antioxidant activity in young wrestlers. *Biological Trace Element Research, 134*(1), 55–63. https://doi.org/10.1007/s12011-009-8457-z

Kloubert, V., & Rink, L. (2015). Zinc as a micronutrient and its preventive role of oxidative damage in cells. *Food & Function, 6*(10), 3195–3204. https://doi.org/10.1039/C5FO00630A

Li, L., Qiu, Z., Dong, H., Ma, C., Qiao, Y., & Zheng, Z. (2021). Structural characterization and antioxidant activities of one neutral polysaccharide and three acid polysaccharides from the roots of Arctium lappa L.: A comparison. *International Journal of Biological Macromolecules, 182*, 187–196. https://doi.org/10.1016/j.ijbiomac.2021.03.177

Li, L., Xu, J. X., Cao, Y. J., Lin, Y. C., Guo, W. L., Liu, J. Y., … Lv, X. C. (2019). Preparation of Ganoderma lucidum polysaccharide-chromium (III) complex and its hypoglycemic and hypolipidemic activities in high-fat and high-fructose diet-induced pre-diabetic mice. *International Journal of Biological Macromolecules, 140*, 782–793. https://doi.org/10.1016/j.ijbiomac.2019.08.072

Liao, W., Lu, Y., Fu, J., Ning, Z., Yang, J., & Ren, J. (2015). Preparation and characterization of dictyophora indusiata polysaccharide–zinc complex and its augmented antiproliferative activity on human cancer cells. *Journal of Agricultural and Food Chemistry*, 63(29), 6525–6534.https://doi.org/10.1021/acs.jafc.5b00614.

Maares, M., & Haase, H. (2020). A guide to human zinc absorption: General overview and recent advances of in vitro intestinal models. *Nutrients, 12*(3), 762.

Mitić, Ž., Cakić, M., Nikolić, G. M., Nikolić, R., Nikolić, G. S., Pavlović, R., & Santaniello, E. (2011). Synthesis, physicochemical and spectroscopic characterization of copper (II)-polysaccharide pullulan complexes by UV–vis, ATR-FTIR, and EPR. *Carbohydrate Research, 346*(3), 434–441. https://doi.org/10.1016/j.carres.2010.12.011

Morcali, M. H. (2015). Reductive atmospheric acid leaching of spent alkaline batteries in H2 SO4/Na2 SO3 solutions. *International Journal of Minerals, Metallurgy, and Materials, 22*(7), 674–681. https://doi.org/10.1007/s12613-015-1121-z

Mothé, C. G., & de Freitas, J. S. (2013). Extraction, purification of cashew polysaccharide and characterization by GC-MS, FTIR, NMR, TG/DTG. *International Journal of Research and Reviews in Applied Sciences, 16*(3), 401–408. https://doi.org/10.52403/ijrr.

Outten, C. E., & O'Halloran, T. V. (2001). Femtomolar sensitivity of metalloregulatory proteins controlling zinc homeostasis. *Science, 292*(5526), 2488–2492. https://doi.org/10.1126/science.1060331

Pories, W., Henzel, J., Rob, C., & Strain, W. (1967). Acceleration of wound healing in man with zinc sulphate given by mouth. *The Lancet, 289*(7482), 121–124. https://doi.org/10.1016/S0140-6736(67)91031-8

Prasad, A. S. (2013). Discovery of human zinc deficiency: Its impact on human health and disease. *Advances in Nutrition, 4*(2), 176–190. https://doi.org/10.3945/an.112.003210

Prasad, A. S., Oberleas, D., Wolf, P., Horwitz, J. P., Collins, R., & Vazquez, J. M. (1967). Studies on zinc deficiency: Changes in trace elements and enzyme activities in tissues of zinc-deficient rats. *The Journal of Clinical Investigation, 46*(4), 549–557. https://doi.org/10.1172/JCI105556

Qiu, Z., Zheng, Z., Zhang, B., Sun-Waterhouse, D., & Qiao, X. (2020). Formation, nutritional value, and enhancement of characteristic components in black garlic: A review for maximizing the goodness to humans. *Comprehensive Reviews in Food Science and Food Safety, 19*(2), 801–834. https://doi.org/10.1111/1541-4337.12529

Rojas, L. X., McDowell, L. R., Cousins, R. J., Martin, F. G., Wilkinson, N. S., Johnson, A. B., & Velasquez, J. B. (1995). Relative bioavailability of two organic and two inorganic zinc sources fed to sheep. *Journal of Animal Science, 73*(4), 1202–1207. https://doi.org/10.2527/1995.7341202x

Rossi, M., Corradini, C., Amaretti, A., Nicolini, M., Pompei, A., Zanoni, S., & Matteuzzi, D. (2005). Fermentation of fructooligosaccharides and inulin by bifidobacteria: A comparative study of pure and fecal cultures. *Applied and environmental microbiology, 71*(10), 6150–6158. https://doi.org/10.1128/AEM.71.10.6150-6158.2005

Shay, N. F., & Mangian, H. F. (2000). Neurobiology of zinc-influenced eating behavior. *The Journal of Nutrition*, 130(5), 1493S–1499S. https://doi.org/10.3390/nu12030762.

Storrie, H., & Stupp, S. I. (2005). Cellular response to zinc-containing organoapatite: An in vitro study of proliferation, alkaline phosphatase activity and biomineralization. *Biomaterials, 26*(27), 5492–5499. https://doi.org/10.1016/j.biomaterials.2005.01.043

Subasi, B. G., Xiao, J., & Capanogluo, E. (2021). Potential use of Janus structures in food applications. eFood, 2(6), 279-287.https://doi.org/10.53365/efood.k/146162.

Sunuwar, L., Medini, M., Cohen, L., Sekler, I., & Hershfinkel, M. (2016). The zinc sensing receptor, ZnR/GPR39, triggers metabotropic calcium signalling in colonocytes and regulates occludin recovery in experimental colitis. *Philosophical Transactions of the Royal Society B: Biological Sciences, 371*(1700), 20150420. https://doi.org/10.1098/rstb.2015.0420

Treanor, C. E., Rich, J. W., & Rehm, R. G. (1968). Vibrational relaxation of anharmonic oscillators with exchange-dominated collisions. *The Journal of Chemical Physics, 48*(4), 1798–1807. https://doi.org/10.1063/1.1668914

Xu, J., Yin, H., Li, Y., & Liu, X. (2010). Nitric oxide is associated with long-term zinc tolerance in Solanum nigrum. *Plant Physiology, 154*(3), 1319–1334. https://doi.org/10.1104/pp.110.162982

Yan, J. K., Wang, C., Yu, Y. B., Wu, L. X., Chen, T. T., & Wang, Z. W. (2021). Physicochemical characteristics and in vitro biological activities of polysaccharides derived from raw garlic (Allium sativum L.) bulbs via three-phase partitioning combined with gradient ethanol precipitation method. *Food Chemistry, 339*, Article 128081. https://doi.org/10.1016/j.foodchem.2020.128081

Yang, J., Rainville, P., Liu, K., & Pointer, B. (2021a). Determination of lactose in low-lactose and lactose-free dairy products using LC-MS. *Journal of Food Composition and Analysis, 100*, Article 103824. https://doi.org/10.1016/j.jfca.2021.103824

Yang, Q., Wang, Y., Yang, M., Liu, X., Lv, S., Liu, B., … Zhang, T. (2021b). Effect of glycation degree on the structure and digestion properties of ovalbumin: A study of amino acids and peptides release after in vitro gastrointestinal simulated digestion. *Food Chemistry, 131331*. https://doi.org/10.1016/j.foodchem.2021.131331

Yousef, M. I., El Hendy, H. A., El-Demerdash, F. M., & Elagamy, E. I. (2002). Dietary zinc deficiency induced-changes in the activity of enzymes and the levels of free radicals, lipids and protein electrophoretic behavior in growing rats. *Toxicology, 175*(1–3), 223–234. https://doi.org/10.1016/S0300-483X(02)00049-5

Yu, Q., Chen, W., Zhong, J., Huang, D., Shi, W., Chen, H., & Yan, C. (2022). Purification, structural characterization, and bioactivities of a polysaccharide from Coreopsis tinctoria. *Food Frontiers*. https://doi.org/10.1002/fft2.145

Zhong, R., Farag, M. A., Chen, M., He, C., & Xiao, J. (2022). Recent advances in the biosynthesis, structure–activity relationships, formulations, pharmacology, and clinical trials of fisetin. *eFood, 3*(1–2), e3.

Zhu, Y., Li, H., Ma, J., Xu, T., Zhou, X., Jia, S., Zha, J., Xue, D., Tao, W., Xiong, Q., Yuan, J., & Chen, J. (2020). A green and efficient deproteination method for polysaccharide from Meretrix meretrix Linnaeus by copper ion chelating aerogel adsorption. Journal of Cleaner Production, 252, 119842. https://doi.org/10.1016/j.jclepro.2019.119842.